Characterization of Second Phase Particles in Twin-Roll Cast Aluminum Alloy AA 8011

Sooraj Patel and Jyoti Mukhopadhyay

Abstract A thin strip of 7 mm thickness was manufactured using a twin-roll casting process. Second phase particles were segregated at the center region during the solidification of aluminum alloy AA 8011. Such segregations played a vital role in the formation of pinholes. In the present work, the microstructural analysis was carried out to study the centerline segregation. Fine equiaxed grains were formed at the surface due to the rapid solidification and dynamic recrystallization. An increase in hardness was attributed to centerline segregation of the second phase particles. β-AlFeSi compounds with needle shape morphology were segregated in the thickness range of 10–20 μm parallel to the twin-roll casting direction. Sub-grains were formed inside the elongated grains due to dynamic recovery. Dispersoids were precipitated after the homogenization, which was not found in the as-received twin-roll cast strip.

Keywords Twin-roll casting · Centerline segregation · Second phase particles · Characterization · Phase transformation

Introduction

Aluminum alloy AA 8011 consists of Fe and Si as major alloying elements. The alloy is also used for making packaging**,** cable wrap, cigarette foils, photographic plates, electrolytic capacitor material, fan blade sheets, lamp cap stocks, aluminum tubes for kitchen ventilators, and flexible air ducts. The usual trend to get thin strip is by hot rolling of DC cast slab. Several hot rolling and annealing steps need to be performed to reduce its thickness. High energy and running costs are associated with these several hot rolled processes followed by cold rolling steps. The intermediate rolling steps are eliminated in twin-roll casting process in which a 7 mm thick strip is directly produced from the molten metal [1].

S. Patel · J. Mukhopadhyay (✉)

Department of Materials Engineering, Indian Institute of Technology Gandhinagar, Ahmedabad, Gujarat 382355, India
e-mail: jm@iitgn.ac.in

Solidification takes place as the molten metal passes through the water-cooled rollers. The solidification phenomenon significantly influences the microstructure of the twin-roll cast alloy. Intermediate thermo-mechanical processing steps are carried out to achieve the required mechanical properties [2, 3]. As-cast aluminum strip is cold rolled to the foil stock gauge thickness, which is followed by annealing at the temperature range of 350–400 °C [2]. The cold rolling process achieves the final thickness of the packaging foil. Usually, the aluminum foils used for the packaging are in O-temper condition.

A detailed analysis of the as-cast aluminum strip is necessary to control the processing conditions and the mechanical properties. In aluminum alloy AA 8011, Fe and Si are much higher than the maximum soluble limit. A binary Al–Fe and ternary Al–Fe-Si phases were formed for the lower and higher silicon content [2, 4–7]. The maximum solubility of Fe in aluminum is very low, nearly 0.05 wt% at 650 °C [8]. Si can dissolve up to 1.65 wt% in aluminum at 577 °C [8]. Solid solution hardening is limited due to the less formation of strengthening precipitates. An excessive Fe present in the aluminum matrix makes intermetallic compounds with Si and Al. Such compounds are agglomerated at the center during solidification and these compounds form centerline segregations [8, 9].

Binary phases such as Al6Fe and Al13Fe4 (θ phase) are formed for low silicon aluminum alloys. The Bravais lattice for the Al6Fe compound is orthorhombic, whereas for Al_3Fe or $Al_{13}Fe_4$ compounds are monoclinic. Al_3Fe forms needle shape morphology that adversely affects the formability of packaging foils [2, 4]. Ternary Al–Fe-Si phases are formed when the Si content exceeds 0.5 wt%. These phases are available in two forms: α-AlFeSi and β-AlFeSi. α-AlFeSi makes compounds of Al_8Fe_2Si and $Al_{12}Fe_3Si_2$ that are in a cubic or hexagonal structure. β-AlFeSi phases such as Al_5FeSi and $Al_9Fe_2Si_2$ are in monoclinic lattice structures [2, 4, 8]. The ratio of Fe and Si is a critical parameter to identify the existing phases in the second phase particles. Atomic and wt% ratio of Fe:Si varies between 2:1 to 3:1 and 4:1 to 6:1, respectively, for the α-AlFeSi phase. On the other hand, the atomic and wt% ratio for β-AlFeSi phase is nearly unity and 2:1, respectively [2].

The intermetallic compounds in the centerline segregation are hard and brittle. Needle-shaped β-AlFeSi phase reduces the formability, and these phases also act as crack initiation sites [10, 11]. β-AlFeSi is transformed into a circular shape (α-phase) when the specimen is homogenized above 550 °C [12]. The coarsening of the second phase is observed with an increase in the homogenization temperature [12]. Monoclinic Al_3Fe/Al_6Fe phases were formed due to the homogenization at higher temperatures [6, 13–15]. The ternary phase diagram of Al–Fe-Si phases is useful to identify the equilibrium phases at different temperatures [12]. The microstructure has been analyzed for the twin-roll cast low-Mg aluminum alloy for different heat treatment conditions. Recovery is prevailing during the low-temperature annealing, whereas recrystallization is dominant for the high-temperature annealing [16].

Significant research has been carried out to analyze the stable and metastable phases in an aluminum matrix during twin-roll casting [11–15]. However, the formation of centerline segregation and agglomeration of the second phase particles need to be studied in detail. The formability decreases with an increase in agglomeration

of the second phase particles. The influence of the centerline segregation on the hardness is essential to estimate the formability. Precipitation of the dispersoids improves the mechanical properties of the aluminum foils [7, 17].

The present work was focused on the formation of centerline segregation and its microstructural characterization in twin-roll cast aluminum alloy AA 8011. Critical analysis of the intermetallic compound was helpful to identify the phases present in the centerline segregation. These phases governed the morphology of the second phase particles. Undesirable needle particles could be transformed into desirable circular/spherical particles by phase transformation of Al–Fe-Si compound from beta to alpha. The rapid cooling during the continuous casting was unfavorable to the dissolution particles. Homogenization followed by slow cooling could form fine dispersoids that could improve the mechanical properties. Dispersoid formation in the as-cast AA 8011 and the analysis of dispersoid precipitation after homogenization were included in the study.

Experimental Procedure

Material and Method

Twin-roll cast aluminum alloy AA 8011 with high Fe (0.6 wt%) and Si (0.62%) was used for the centerline segregation analysis. The remaining elements were Cu, Mn, Mg, and Ti, minor in concentration (< 0.05 wt%). AA 8011 strip of 7 mm thickness was taken for the investigation in the as-cast condition. The molten metal was preheated to 800 °C in the holding furnace before pouring. The headbox temperature before passing the molten metal between the cooling rollers was kept at 700 ± 5 °C. The molten metal was fed at a constant rate of 0.9 m/min.

The specimen was homogenized at 575 °C to study the phase transformation for centerline segregation. Homogenization was carried out using a Nabertherm high-temperature furnace. The specimen was heated from room temperature to 575 °C in 2.5 h. The heating rate was kept low to ensure the thermal equilibrium between the specimen and furnace. The furnace was held at 575 °C for 8 h, and then it cooled up to room temperature within 9 h.

The microstructure of the twin-roll cast aluminum alloy AA 8011 was studied to examine the formation of centerline segregation. The distribution analysis of the Al–Fe-Si second phase particles inside the centerline segregation was carried out using Scanning Electron Microscopy (SEM) with Wavelength Dispersive Spectroscopy (WDS). The phases were identified based on the morphology and Fe:Si ratio using the Energy Dispersive Spectroscopy (EDS). Vickers hardness was measured across the cross-section of the twin-roll cast AA 8011. Dislocations and sub-grain formation inside elongated grains were investigated in the as-cast aluminum strip. The location of intermetallic compounds was recognized using Transmission Electron Microscopy (TEM).

## *Microstructure and Hardness Evaluation*

The specimen was cut in 15 mm × 7 mm × 10 mm size using an abrasive cutter. Rough polishing was carried out using silicon carbide grit papers of sizes varying from P220 to P2500. Final polishing was performed on a single disc polishing machine using 6, 3, and 1 μm diamond paste applied on the polishing cloth. Ethanol was kept as a medium during the final polishing. The specimen was etched using Keller's reagent (95 mL water, 2.5 mL HNO_3, 1.5 mL HCl, 1.0 mL HF). The microstructure was revealed by varying the concentration of HCl and HNO_3. The microstructure was obtained at the cross-section near the surface.

Micro-hardness variation throughout the cross-section was measured using Vickers hardness tester, as shown in Fig. 1. It was measured at every 100 μm distance on the thickness section starting from one end. The load of 100 g was applied for 20 s at each indentation point.

Scanning Electron Microscopy (SEM) was carried out using JEOL (JSM 7600F) to characterize the second phase particles inside the centerline segregation. Such particles were difficult to observe using optical microscopy. Elemental analysis was performed using EDS attachment (Oxford, Model INCA Energy 250 EDS). The phases were identified based on morphology and chemical composition. WDS attachment analyzed the distribution of second phase particles. Specimen preparation for SEM was similar to the process used for optical microscopy, where the specimen was polished using 1 μm diamond paste.

Transmission Electron Microscopy was used to characterize as-cast AA 8011 and the specimen was homogenized at 575 °C for 8 h. TEM imaging and analysis were carried out using a 300 kV FE-TEM (FEI make, Tecnai G2 F30 model). An initial specimen was cut into 15 mm × 7 mm × 8 mm using an abrasive cutter. A precision wire saw was used to cut a thin slice of 500 μm from the initial specimen. The wire used in the instrument was made from steel embedded with fine diamond particles. For rough polishing, silicon carbide abrasive grit papers (P600 and P800) were used to reduce the slice thickness from 500 μm to 200 μm. A small disc of 3 mm diameter was punched out using a disc punch. The specimen dimension after punching out the disc was Ø3 mm × 200 μm. The thickness was reduced from 200 to 100 μm by fine grit abrasive papers (P1000, P1200, and P2500) using a disc grinder. Then the specimen was subjected to the dimpling process, where fine alumina and diamond suspensions were used as abrasive medium. The thickness of the disc specimen was

Fig. 1 Schematic of Vickers hardness measurement
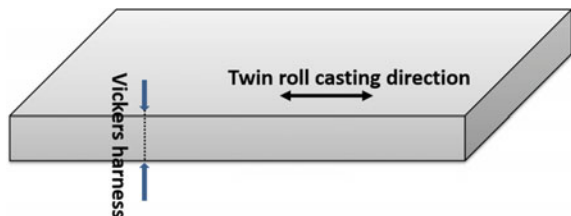
reduced to 20 μm at the center region using the dimple grinder. The ion mill further thinned the specimen from 20 μm to 200 nm at the center area. The final specimen dimension for the TEM analysis was Ø3 mm × ~200 nm. The microstructural analysis and dispersoid precipitation after homogenization were studied using TEM.

Results and Discussion

Optical Microscopy

The twin-roll cast aluminum alloy microstructure was significantly different from that of the rolled or annealed plates. The dynamic processes and solidification phenomenon influenced the microstructure in twin-roll cast strips. Very fine equiaxed grains followed by the columnar grains were observed on the cross-section near the surface, as shown in Fig. 2a. Equally distributed molten metal passing from the headbox came in contact with water-cooled rollers. The surface was solidified quickly as it was in direct contact with the cooling rollers compared to the interior. The solidified surface underwent plastic deformation further during the twin-roll casting process. The temperature of the just solidified region at the surface was sufficiently higher that could form the new grains at the same time. Therefore, recrystallization of the just solidified surface took place along with the hot deformation. As a result, very fine equiaxed grains were formed due to dynamic recrystallization. Such fine grains with high angle grain boundaries at the surface were also observed earlier by Yücel Birol [3, 18] for Al–Fe-Si and Al–Fe–Mn–Si alloys. The columnar grains were found next to the fine equiaxed grains as solidification was progressed from the surface to the center region.

The alloying elements such as Fe and Si remain undissolved during the solidification when such elements are beyond the maximum solubility limit. These particles

Fig. 2 **a** Microstructure of twin-roll cast AA 8011 near the surface **b** centerline segregation

Cross-sectional view near to surface

Segregation at the center
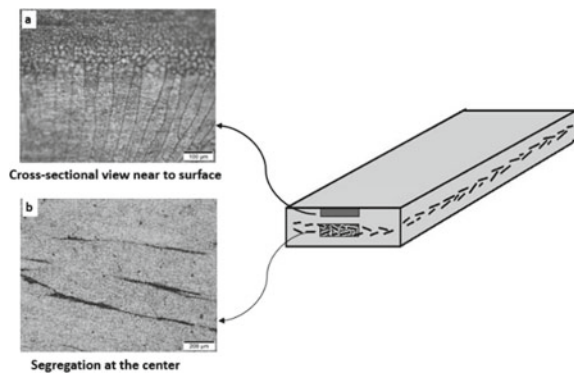
travel along the columnar grains from the surface towards the center during the directional solidification process. The macro-segregation of the intermetallic compound occurred due to the movement of micro-segregation along with the motion of the liquid and free crystals. The micro-segregation moved inward easily through the columnar grains and segregated at the center region. The centerline segregation of the second phase particles is shown in Fig. 2b. Such macro-segregations were dominant for the higher columnar zone. As Ghosh [19] mentioned earlier, the macro-segregation of intermetallic compounds could be reduced if such columnar grains were converted into equiaxed grains.

Vickers Hardness

The hardness distribution throughout the thickness is shown in Fig. 3. The microstructural variation led to the non-uniform hardness values. The surface region was harder than that of the interior. The micro-hardness near both surface ends was nearly 50 HV, whereas the interior was in the range of 42–44 HV. Rapid solidification and dynamic recrystallization formed equiaxed grains of almost in the size range of 5–10 μm at the surface. The formation of fine grains led to an increase in hardness values at both surface ends. A peak hardness value of 62.1 HV was identified nearly at 4.5 mm from one end. The intermetallic compounds present in the centerline segregation increased the hardness, as shown in Fig. 3. However, the exact hardness of the centerline segregation could not be measured as the indentation size was more than the width of the segregation.
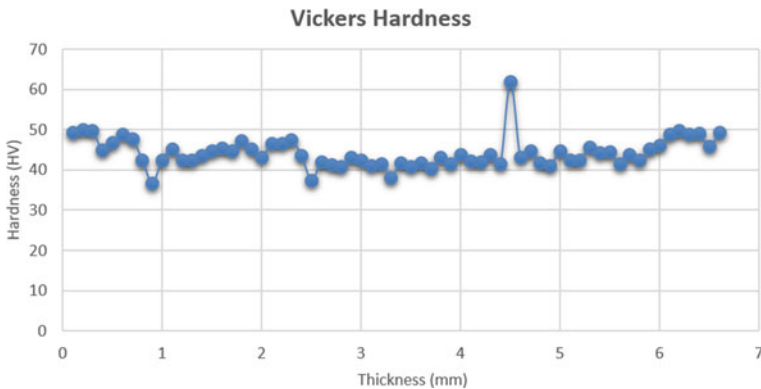

Fig. 3 Micro-hardness variation across the thickness section

Scanning Electron Microscopy

The segregation of second phase particles was studied using back-scattered mode in SEM, and the elemental analysis of the second phases was carried out using EDS attachment. The second phase particles were segregated parallel to the twin-roll casting direction and agglomerated in a 10–20 μm thickness range in particular segregation. One of the segregations identified near the center is shown in Fig. 4a. Furthermore, the magnified images of the centerline segregation are shown in Fig. 4b and c, respectively. These second phase particles were in needle shape morphology, and they were oriented towards the centerline segregation direction.

Fe-based phases were present in the aluminum matrix as the solubility of Fe in Al was very low. Ternary phase diagram showed that monoclinic phase Al3Fe was stable for the low silicon aluminum alloy, whereas β-phase was stable for the high silicon content exceeding 0.5 wt% irrespective of the temperature [12]. Elemental analysis was carried out to identify the Fe and Si content of the second phase particles. The quantitative analysis performed on one of the particles is shown in Fig. 5. The Fe:Si ratio of the needle-shaped particles in wt% and atomic% was approximately 2:1 and unity, respectively. Similar features have been reported earlier for the β-phase of the Al–Fe-Si compound [2, 4, 12]. β-phase formed the needle shape morphology with the chemical composition of $Al_5FeSi/Al_9Fe_2Si_2$ [8].

The distribution of the second phase particles was observed using WDS attachment with the SEM. The line scan was performed across one of the centerline segregations as shown in Fig. 6a. The distribution of Al, Fe, and Si content throughout the segregation width is shown in Fig. 6b, c, and d, respectively. Both Fe and Si content peaks were observed from 1 to 7 μm width in Fig. 6c, d. Accordingly, less concentration of aluminum content was found in that region in Fig. 6b due to the higher concentration of Fe and Si. Similar peaks of Fe and Si contents were also
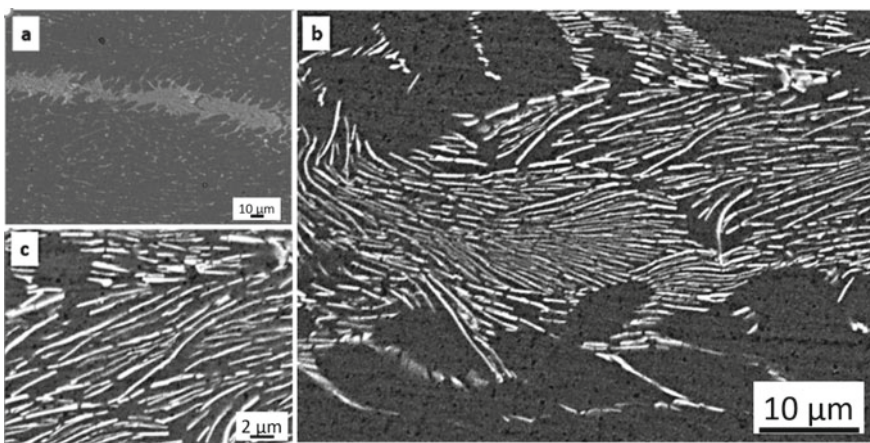
Fig. 4 Needle-shaped second phase particles in centerline segregation of twin-roll cast AA 8011
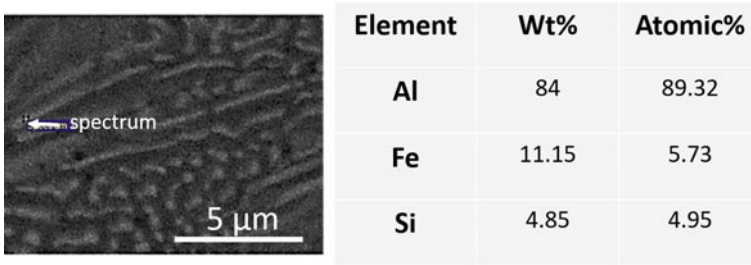
Element	Wt%	Atomic%
Al	84	89.32
Fe	11.15	5.73
Si	4.85	4.95

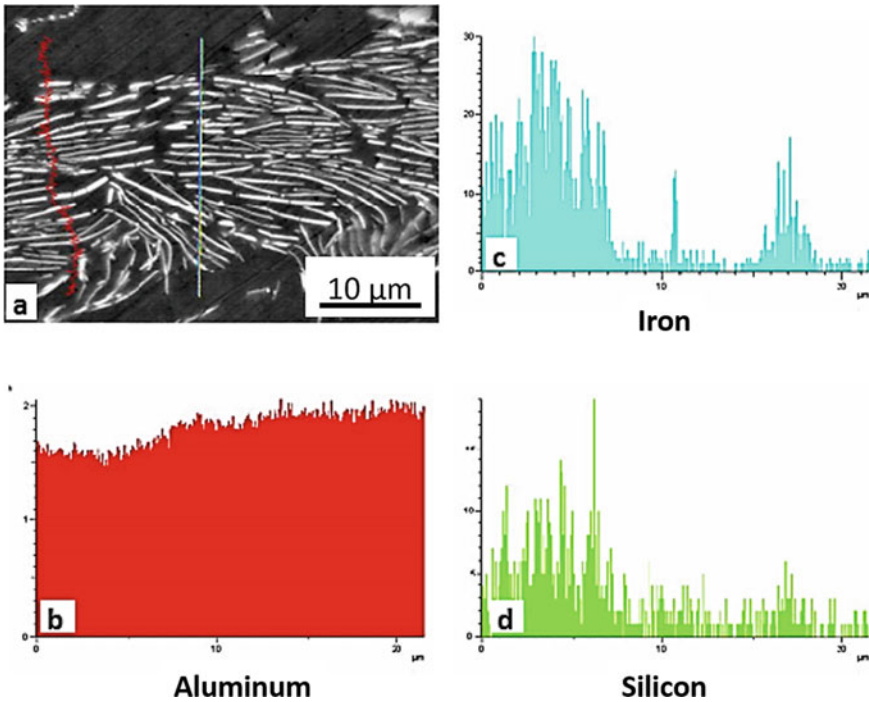**Fig. 5** Elemental analysis of the second phase particles of twin-roll cast AA 8011

**Fig. 6** Distribution of Al, Fe, and Si throughout the segregation

observed in between 15 and 18 µm width. The presence Al–Fe-Si compound can be confirmed due to the concentration of both Fe and Si in particular ranges. β-AlFeSi was found to be a stable phase for the higher silicon-containing aluminum alloys [4].

During twin-roll casting, the equilibrium phases sometimes could not be formed during the experiments because of a higher solidification rate [20, 21]. The chemical composition of metastable phases was different than the stable equilibrium phases. Therefore, the Fe:Si ratio could not remain uniform throughout the line scan. The peak of Fe content was observed at 10.5 µm, as shown in Fig. 6c. Such peak was missing in Si content at the particular location. Therefore, the compound of only Al

and Fe was present at 10.5 μm. The needle-shaped monoclinic Al_3Fe intermetallic phase was earlier observed for low silicon aluminum-based alloys [4]. Apart from the stable Al_3Fe phase, metastable phases such as Al_6Fe and $Al_{13}Fe_4$ were also common [2]. Such phases might be present at the width of 10.5 μm. It was challenging to differentiate β-AlFeSi and Al_3Fe phases from the microscopy images, since bot**h** phases formed needle-shaped particles.

Transmission Electron Microscopy

The region near the centerline segregation was analyzed using transmission electron microscopy. TEM images of as-cast aluminum alloy AA 8011 are shown in Fig. 7. The initial material was in the molten stage, which was subsequently solidified between
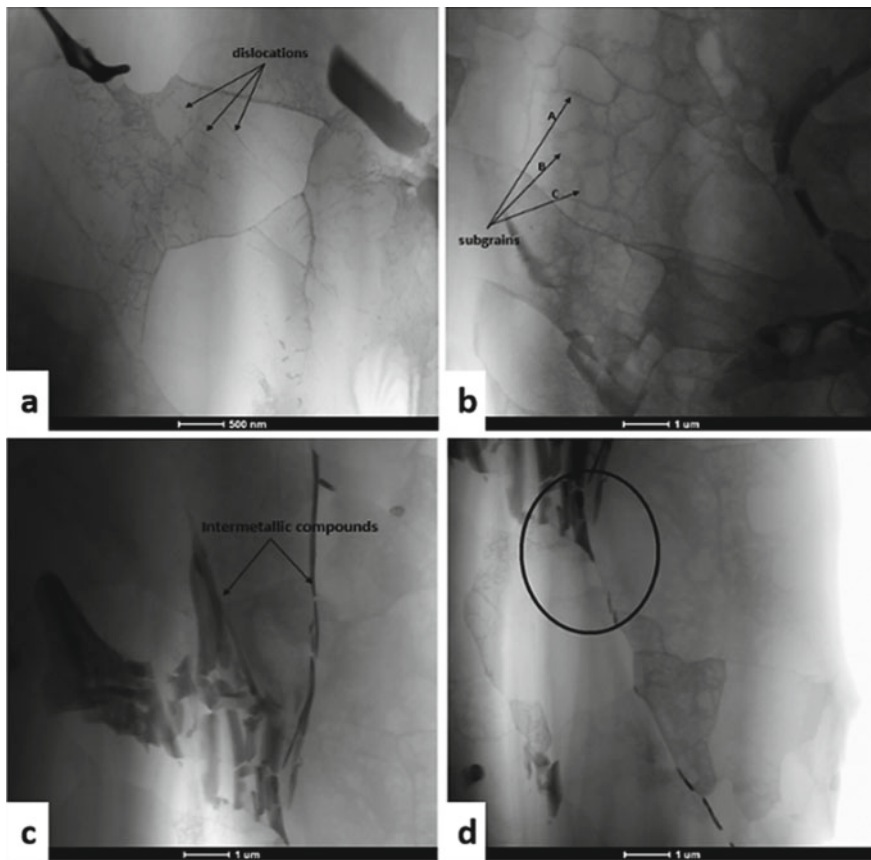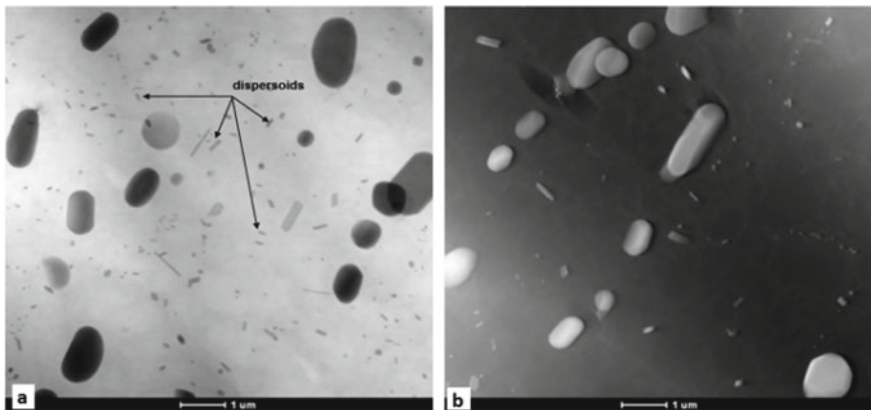

Fig. 7 TEM of twin-roll cast AA 8011

the rollers. The line defects were generated in crystal lattice during the solidification. Dislocations formed inside the grains are shown in Fig. 7a. Both cross slip and the climb were easy for high stacking fault energy materials such as aluminum. Sub-grains were continuously formed inside the elongated grains due to the dynamic recovery as shown in Fig. 7b. Dislocation annihilation occurred due to the migration of dislocations towards the sub-grain boundary. Therefore, dislocation-free well-developed sub-grains were formed, as shown in Fig. 7b (sub-grain—A). Sub-grain boundaries were in the developing phase via dislocation migration in the remaining sub-grains such as B, C, and others. High dislocation density was still observed on the right side of the elongated grain as the sub-grains were not formed.

The needle-shaped second phase particles observed using SEM were also found in TEM images. The agglomeration of such intermetallic compounds is shown in Fig. 7c. Such particles were stabilized at the grain boundary interface, as shown in Fig. 7d. These particles led to intergranular cracking and weakened the grain boundaries that adversely affect the mechanical properties.

Figure 8 shows the TEM images of the homogenized specimen at temperature 575 °C. Circular-shaped second phase particles were formed when the specimen was homogenized at a higher temperature for a sufficiently long time. Some needle-shaped intermetallic particles were also present, as shown in Fig. 8b.

The Fe, Si, and other constituent phases might be dissolved in the aluminum matrix when the material was in the molten stage. The rapid solidification during the twin-roll casting process might not allow the formation of such phases. High-temperature homogenization followed by slow cooling gave sufficient energy and time to precipitate the fine intermetallic phases, called dispersoids. Needle-shaped fine dispersoids formed during the homogenization are shown in Fig. 8. These disper-soids were uniformly distributed throughout the specimen that gave uniform properties of aluminum foils. Such dispersoids were not observed in the as-received


Fig. 8 TEM after homogenization at 575 °C

twin-roll cast AA 8011 strip. These fine particles offered dispersion hardening and improved the mechanical properties of the material.

A semi-quantitative elemental analysis of the second phase particles was performed using EDS attachment, as shown in Fig. 9. The chemical compositions of the circular- and needle-shaped particles and a region without intermetallic phases are shown in Table 1a, b, and c, respectively. Various chemical composition were identified for the different morphological phases. The Fe:Si ratio for the circular/spherical phase was nearly 4:1 and 2:1 in wt% and atomic%, respectively (Table 1a). Similarly, the Fe:Si ratio was earlier reported for the α-phase of the AlFeSi compound with the same morphology [2, 4]. Furthermore, the α-AlFeSi phase was a stable equilibrium phase for the 0.6 wt% silicon at the higher temperature [12]. Therefore, the α-AlFeSi compound was confirmed for the circular particles found after homogenization.

Needle shape second phases were still observed after homogenization at 575 °C. However, the size and aspect ratio of the needle-shaped particles were significantly less than the as-received twin-roll cast specimen. These particles might be

Fig. 9 Elemental analyses of second phase particles in specimen homogenized at 575 °C for 8 h
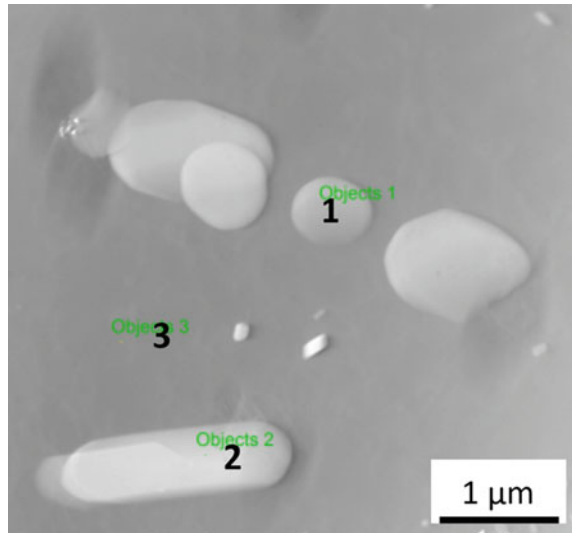
Table 1 Elemental analyses of circular intermetallic particle (a), needle-type intermetallic particle (b), and without intermetallic region (c)

(a) Object 1			(b) Object 2			(c) Object 3		
Element	Wt%	Atomic%	Element	Wt%	Atomic%	Element	Wt%	Atomic%
Al	85.32	90.89	Al	64.30	74.54	Al	99.89	99.9
Fe	11.63	5.98	Fe	25.83	14.47	Fe	–	–
Si	3.05	3.12	Si	9.87	11.00	Si	0.11	0.10

precipitated in the form of dispersoids, and particle-coarsening occurred due to high-temperature homogenization for a sufficiently long exposure time. The Fe:Si ratio of the needle-type intermetallic particle was below 3:1 and just above unity in wt% and atomic%, respectively (Table 1b). Here, the particles were still in the needle shape, but the aspect ratio was very small compared to the as-received twin-roll cast specimen. Therefore, β-AlFeSi or other metastable phases other than the α-AlFeSi were present in the needle-shaped particle. A negligible silicon content was identified in the aluminum matrix in the region without intermetallic phases (Table 1c).

Conclusion

1. Very fine equiaxed grains followed by columnar grains were observed at the surface during the twin-roll casting process. Dynamic recrystallization and the solidification structure formed fine equiaxed grains near the surface.
2. The surface of the as-cast strip was harder than the interior. A sharp peak in hardness was attributed to the centerline segregation.
3. The movement of micro-segregated particles along with columnar grains formed centerline segregation.
4. Sub-grains were formed inside the elongated grains due to easy climb or cross slip for high stacking fault energy materials such as aluminum. Well-developed dislocation-free sub-grains were observed due to the migration of dislocations towards the sub-grain boundary.
5. Needle-shaped second phase particles (β-AlFeSi) were found inside the centerline segregation. These particles were closely agglomerated parallel to the twin-roll casting direction.
6. Dispersoids were formed when the specimen was homogenized at 575 °C. Such dispersoids were not found in as-received twin-roll cast specimens. α-AlFeSi phase with the circular/spherical shape morphology was identified for the homogenized specimen.

References

1. Cook R, Grocock PG, Thomas PM, Edmonds DV, Hunt JD (1995) Development of the twin-roll casting process. J Mater Process Tech 55:76–84. https://doi.org/10.1016/0924-0136(95)01788-7

2. Lentz M, Laptyeva G, Engler O (2016) Characterization of second-phase particles in two aluminium foil alloys. J Alloys Compd 660:276–288. https://doi.org/10.1016/j.jallcom.2015.11.111

3. Birol Y (2008) Response to annealing treatments of twin-roll cast thin Al-Fe-Si strips. J Alloys Compd 458:265–270. https://doi.org/10.1016/j.jallcom.2007.04.048

4. Allen CM, O'Reilly KAQ, Cantor B, Evans PV (1998) Intermetallic phase selection in 1XXX Al alloys. Prog Mater Sci 43:89–170. https://doi.org/10.1016/S0079-6425(98)00003-6

5. Skjerpe P (1987) Intermetallic phases formed during DC-Casting of an Al-0.25wt pct Si alloy. Mettalurgical Trans A 18a:189–190

6. Tanihata H, Sugawara T, Matsuda K, Ikeno S (1999) Effect of casting and homogenizing treatment conditions on the formation of Al-Fe-Si intermetallic compounds in 6063 Al-Mg-Si alloys. J Mater Sci 34:1205–1210. https://doi.org/10.1023/A:1004504805781

7. Shakiba M, Parson N, Chen XG (2014) Effect of homogenization treatment and silicon content on the microstructure and hot workability of dilute Al-Fe-Si alloys. Mater Sci Eng A 619:180–189. https://doi.org/10.1016/j.msea.2014.09.072

8. Kumar R, Gupta A, Kumar A, Chouhan RN, Khatirkar RK (2018) Microstructure and texture development during deformation and recrystallisation in strip cast AA8011 aluminum alloy. J Alloys Compd 742:369–382. https://doi.org/10.1016/j.jallcom.2018.01.280

9. Sanders RE, Hollinshead PA, Simielli EA (2004) Industrial development of non-heat treatable aluminum alloys. Mater Forum 28:53–64.

10. Ryu JH, Lee YS, Lee DN (2001) The effect of precipitation on the evolution of recrystallization textures in an AA 8011 aluminum alloy sheet. Met Mater Int 7:251–256. https://doi.org/10.1007/bf03026983

11. Shoji R, Fukijura C (1990) Precipitation of Fe and Si in cold rolled Al-Fe-Si sheet during annealing. Mech Corros Prop Ser A Key Eng Mater 44–45:163–180. https://doi.org/10.4028/www.scientific.net/kem.44-45.163

12. Patel S, Mukhopadhyay J (2019) Effect of homogenization on Al-Fe-Si centerline segregation of twin-roll cast aluminum alloy AA 8011. https://doi.org/10.1007/978-3-030-05864-7_44

13. Li YJ, Arnberg L (2004) A eutectoid phase transformation for the primary intermetallic particle from Alm(Fe, Mn) to Al3(Fe, Mn) in AA5182 alloy. Acta Mater 52:2945–2952. https://doi.org/10.1016/j.actamat.2004.02.041

14. Khalifa W, Samuel FH, Gruzleski JE (2003) Iron intermetallic phases in the Al corner of the Al-Si-Fe system. Metall Mater Trans A Phys Metall Mater Sci 34:807–825. https://doi.org/10.1007/s11661-003-1009-9

15. Rivlin VG, Raynor GV (1980) 3: Critical evaluation of constitution of aluminium-chromium-iron system. Int Met Rev 25:139–157. https://doi.org/10.1179/imtr.1980.25.1.139

16. Tripathi A, Samajdar I, Nie JF, Tewari A (2016) Study of grain structure evolution during annealing of a twin-roll-cast Mg alloy. Elsevier B.V. https://doi.org/10.1016/j.matchar.2016.02.019

17. Engler O, Laptyeva G, Wang N (2013) Impact of homogenization on microchemistry and recrystallization of the Al-Fe-Mn alloy AA 8006. Mater Charact 79:60–75. https://doi.org/10.1016/j.matchar.2013.02.012

18. Birol Y (2009) Response to annealing treatment of a twin-roll cast thin AlFeMnSi strip. J Mater Process Technol 209:506–510. https://doi.org/10.1016/j.jmatprotec.2008.02.019

19. Ghosh A (2001) Segregation in cast products. Sadhana Acad. Proc Eng Sci 26:5–24. https://doi.org/10.1007/BF02728476

20. Li YJ, Arnberg L (2004) Solidification structures and phase selection of iron-bearing eutectic particles in a DC-cast AA5182 alloy. Acta Mater 52:2673–2681. https://doi.org/10.1016/j.actamat.2004.02.015

21. Goulart PR, Lazarine VB, Leal CV, Spinelli JE, Cheung N, Garcia A (2009) Investigation of intermetallics in hypoeutectic Al-Fe alloys by dissolution of the Al matrix. Intermetallics 17:753–761. https://doi.org/10.1016/j.intermet.2009.03.003